Wind erosion on Mars exposes ideal targets for sample return

Mackenzie Day[1]*, William Anderson[2]

[1]University of California Los Angeles, Department of Earth, Planetary, & Space Sciences.

[2]The University of Texas at Dallas, Department of Mechanical Engineering.

[*]Corresponding author: Mackenzie Day (daym@epss.ucla.edu)

Key Points:

- Large eddy simulation was used to model wind-driven surface shear stress across the Jezero crater western delta
- Locations of high shear stress correlate with locations of recent aeolian erosion, a key consideration in sample selection
- Based on two previously interpreted wind regimes, recently-exposed strata are discussed as potential sampling sites

Abstract

The Mars 2020 rover will land in Jezero crater, characterize the local geology, and collect samples to be sent back to Earth. Ionizing radiation at the martian surface degrades the complex organic molecules sought by this mission, making it critical to mission success that samples be selected from recently eroded strata minimally exposed to surface radiation. Erosion on modern Mars is driven by wind. We used numerical modeling to identify sites near the rover landing area where recent aeolian erosion has likely occurred. Large eddy simulation of turbulent airflow over topography was coupled with interpretations of the surface geology to characterize wind-driven erosion across the Jezero crater delta deposit. We discuss potential sediment sources that could drive abrasion and calculate the largest grains mobilized by typical winds over the study area. Our results identify several locations likely eroded by recent winds that provide optimal sites for sample collection.

Plain Language Summary

The Mars 2020 rover will land in Jezero crater and collect samples that will eventually be returned to Earth. Rocks exposed at the surface of Mars become damaged by radiation, therefore, the best samples to collect will be those that have recently been exposed to the surface. On Mars, surface erosion is mostly caused by wind. In this work, we use numerical modeling of wind over the terrain in the Mars 2020 landing area to predict where the landscape has most recently been eroded and identify potential locations for optimal sample collection.

1 Introduction

The Mars 2020 mission will provide unprecedented information about the geology and history of Mars with the ultimate goal of selecting samples to be returned to Earth. The planned landing site in Jezero crater, which includes ancient delta deposits, represents an attractive location for sampling because of the diverse mineralogy in the study area (Goudge et al., 2015; Salvatore et al., 2018) and the potential habitability of the crater's ancient lake (Fig. 1; Fassett & Head, 2005; Schon et al., 2012). Lake and delta sedimentary rocks can preserve complex biomolecules; therefore, samples collected in Jezero crater will offer an exceptional opportunity to look for evidence of ancient life on Mars (Ehlmann et al., 2008). However, the fidelity of any preserved biosignatures will depend on how recently they have been exposed to surface ionizing radiation (Dartnell et al., 2007, 2014), and the recency of erosional exposure on modern Mars depends entirely on the wind. Wind has eroded ~3 km^3 of strata from the Jezero delta deposit (Goudge et al., 2017), but not uniformly, because turbulent interactions between wind and topography cause some regions to erode preferentially over others (Anderson & Day, 2017). Therefore, a thorough understanding of how wind responds to the landscape is essential for identifying sampling locations that have been recently exposed and have the highest biosignature preservation potential.

To date, orbitally-acquired images have provided a glimpse of the complexity of surface-wind interactions in the landing area. Previous work on wind-formed surface geology interpreted two distinct wind regimes that have influenced the landing area (Chojnacki et al., 2018; Day & Dorn, 2019). Erosional linear features called 'yardangs' cross-cut the crater floor and delta deposit, reflecting an era in which southwesterly winds eroded the surface and removed delta strata. Meanwhile, wind streaks and wind-formed bedforms reflect more recent easterly winds.

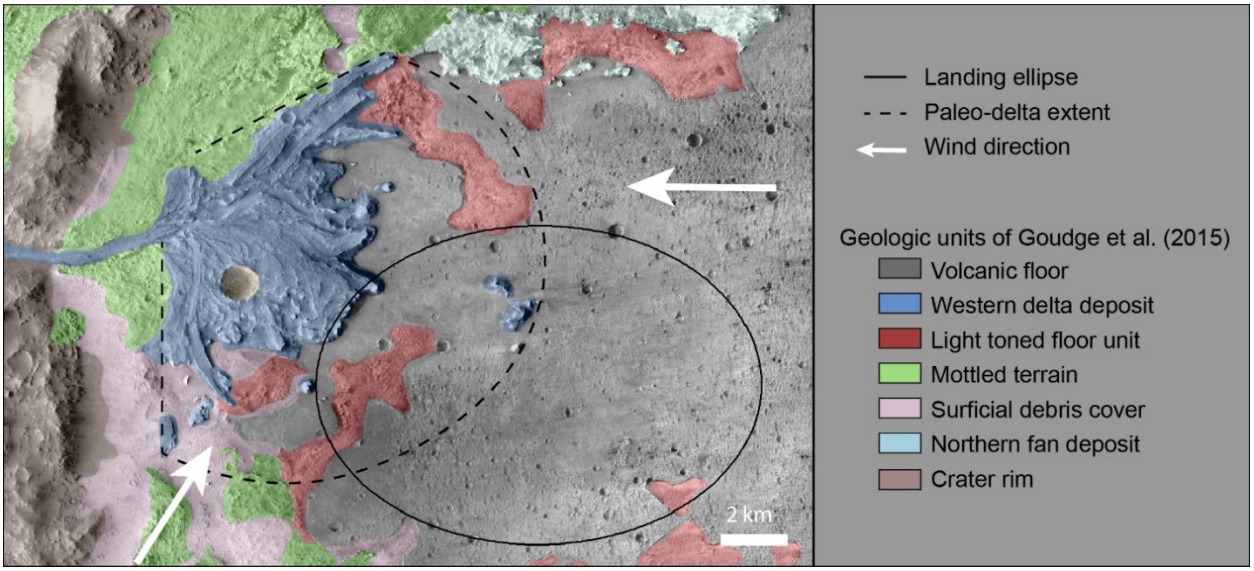

Figure 1: Mars 2020 rover landing area in Jezero crater, Mars. The rover *Perseverance* will land just southeast of a large remnant delta deposit emplaced in an ancient lake. The delta deposit was once much more extensive (dashed line), but has been eroded by wind. Two wind directions have influenced the landscape (arrows), and each indicates different potential optimal sampling locations. Geologic mapping of the area is provided for context.

Intuitively, recent winds should dictate the locations of recent erosion. However, the current supply of sediment in the area is low, and it remains unclear whether modern easterly or older southwesterly winds are responsible for the observed erosion of the delta deposits.

In this work, we leverage computational methods for simulation of realistic turbulent flow over the delta topography to identify erosion patterns on the delta deposit inferred from two different wind directions. The results highlight locations of recent erosion where the newly exposed strata have experienced minimal surface radiation. Samples collected in these areas will have the highest chance of preserving un-degraded biosignatures. Erosion is only possible when sediment is available to cause abrasion, and using the simulation results, we further calculate the largest grain sizes expected to be mobile under typical martian winds. Surface change on modern Mars is dominated by wind, therefore, considering the context of surface-wind interactions will be critical to the mission objectives of characterizing the formation and modification of the geologic record and identifying locations with high potential for preservation of biosignatures.

2 Materials and Methods

Large-eddy simulation (LES) was used to model turbulent atmospheric surface layer flow over topography of the delta proximal to the Mars 2020 landing ellipse. Input topography was derived from a digital elevation model (DEM) provided by the High Resolution Imaging Science Experiment (McEwen et al., 2007). To make the computation tractable, the 1 m/px DEM was down-sampled to a resolution of 100 m/px. Elevation values were clipped to the mapped extent of the delta deposit with margin to ensure that scarps on the edge of the deposits were captured. The area beyond the delta was set to a reference elevation for continuity in the model. In one simulation, the delta was subjected to unidirectional atmospheric forcing from the southwest, and in the second simulation to forcing from the east. The velocity field is modeled as

incompressible, and the viscous stresses are neglected, owing to the very high Reynolds number typical of such large-scale flows (Wyngaard, 2010). With this, evolution of velocity is regulated by the following system of equations,

$$\frac{\partial \widetilde{\boldsymbol{u}}}{\partial t} + \widetilde{\boldsymbol{u}} \cdot \nabla \widetilde{\boldsymbol{u}} = -\frac{1}{\rho}\nabla \tilde{p} - \nabla \cdot \boldsymbol{\tau} + \boldsymbol{e}_x \Pi + \boldsymbol{f}_b \quad \text{and} \quad \nabla \cdot \widetilde{\boldsymbol{u}} = 0, \tag{1}$$

where $\widetilde{\boldsymbol{u}}$ is the velocity vector and "tilde" denotes the grid-filtering operation (Pope, 2000), ρ is density, $\nabla \tilde{p}$ is a pressure correction imposed to maintain the incompressibility condition, $\nabla \cdot \widetilde{\boldsymbol{u}} = 0$, Π is a pressure correction aligned in the streamwise (x) direction, and $\boldsymbol{f}_b$ is a body force included to represent the presence of topographic undulations within Jezero crater. The LES code was originally used for idealized terrestrial atmospheric boundary layer (ABL) turbulence studies (Albertson & Parlange, 1999), but has now been used in a variety of studies, including applications to the ABL on Mars (Anderson & Day, 2017; Day et al., 2016). During simulation, Equation (1) is solved numerically, with horizontal and vertical gradients assessed in Fourier and physical space, respectively. Simulations are advanced until stationarity is attained with respect to flow quantities including kinetic energy; the simulations are subsequently continued for the purpose of recovering turbulence statistics, which regulate the spatial distributions of aerodynamic surface stress used for this article.

The body force term, $\boldsymbol{f}_b$, is evaluated using an immersed-boundary method (IBM), which has been used in a variety of complementary research efforts in high Reynolds number ASL flows over topographic undulations (Anderson, 2013; Anderson & Meneveau, 2010). The grid-filtered turbulent stresses, $\boldsymbol{\tau} = \widetilde{\boldsymbol{u}'\otimes\boldsymbol{u}'}$, where $\boldsymbol{u}'$ denotes fluctuation from the grid-filtered flow (Meneveau & Katz, 2000). In this article, $\nabla \cdot \boldsymbol{\tau}$ is evaluated with the eddy-viscosity concept; a novel closure based open averaging over Lagrangian fluid pathlines is used during LES, which is ideal for the present application wherein topographic relief within Jezero induces large-scale spatial heterogeneities that preclude averaging based on the existing of spatial homogeneity.

To determine an upper bound on the size of grains that would be mobilized by modeled winds, we dimensionalized the shear stress distributions following the methods established in the authors' previous work (Day et al., 2016). Taking advantage of the definition of shear stress, we multiplied the dimensionless basal shear stress output by LES simulations by typical values of atmospheric density and surface shear velocity:

$$\tau_b = \tau_{LES}\, \rho_{atm}\, u_*^2 \tag{2}$$

where ρ_{atm} is the density of the atmosphere, taken as 0.02 kg/m^3. The basal shear velocity relates to a measured wind speed via the law of the wall:

$$u_* = \frac{U(z)\kappa}{\log\left(\frac{z}{z_0}\right)} \tag{3}$$

where κ is the von Kármán constant, $U(z)$ the wind speed at height z, and z_0 the roughness length scale, here taken to be 300 μm. Based on data collected by the InSight lander (Banfield et al., 2020), we assume typical martian winds of U = 5 m/s, at the height of z = 1.665 m.

Grains move when the wind exceeds a threshold needed to initiate particle motion. On Mars, the threshold of motion is much lower if saltation has already begun. The hysteresis between initial and continued motion of sand grains on Mars gives rise to a lower threshold of motion, approximated analytically as (Kok, 2010):

$$u_{*threshold} = c_1 \left(\frac{700}{P}\right)^{\frac{1}{6}} \left(\frac{220}{T}\right)^{\frac{2}{5}} \exp\left(\left(\frac{c_2}{D}\right)^3 + c_3 D^{\frac{1}{2}} - c_4 D\right) \qquad (4)$$

where P is the surface pressure, and T the temperature, here modeled as 200 K and 1000 Pa. D is the grain size of the particle. To determine the largest grain size mobilized by the wind (Fig. 2c,d), we compare this hysteretic threshold to the shear velocities derived from LES. At each grid space, we compared the modeled shear velocity with the curve in Eq. (4) and identified the largest value of D for which $u_{*LES} > u_{*threshold}$. Smaller grains are presumed to be mobile as well, but the D values shown in Figure 2 present upper bounds on mobility and lower bounds on grains in locations of observed immobility.

3 Results

3.1 Surface stress derived from large eddy simulation

Two large eddy simulations were conducted to model turbulent airflow from either the east (Fig. 2a) or southwest (Fig. 2b) interacting with the delta topography (Fig. 2e). Simulations provided instantaneous vector fields of wind across the delta that can be used to study vorticity, shear stress, and turbulent structures. Here, we focus on the imposed surface shear stress as a proxy for the tendency of the wind to cause erosion (e.g., Anderson et al., 1991). The magnitude of shear stress is proportional to the size of sand grains that can be moved and the volume capacity of sediment that can be transported by the wind (e.g., Kok, 2010; Martin & Kok, 2017; Shao & Lu, 2000). Erosion occurs when mobile sediment impacts a surface, causing material removal by abrasion. Thus, holding rock type, sediment supply, and atmospheric conditions constant, shear stress can be used to identify where a surface has been subject to the strongest erosion. A map of shear stress is therefore, a proxy map of where strata have been most recently exposed. The non-linearities in turbulent flow over complex topography require the use of high-fidelity modeling to characterize how wind responds to the surface (Pope, 2000). A time-averaged representation of the surface shear stress from the large eddy simulations is shown in Figure 2. The shear stress has been normalized by the mean value, such that a value of 1 represents the mean, time-averaged surface stress for the region, and values >1 represent stresses above the mean.

3.2 Locations of recent significant erosion

The simulations highlight a number of regions where high shear stress indicates that recent erosion would have taken place. Shear stress is maximized along steep topography where

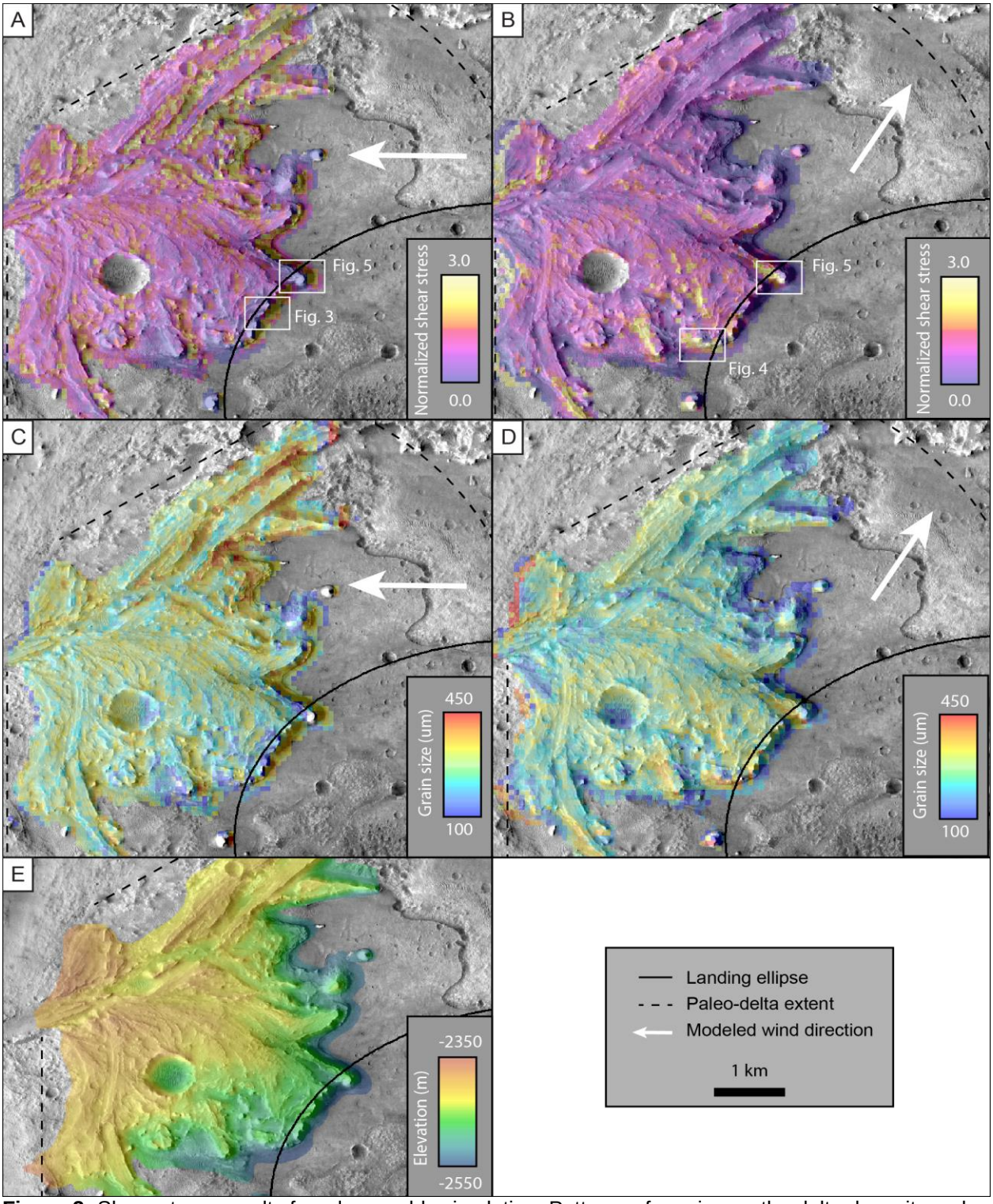

Figure 2: Shear stress results from large eddy simulation. Patterns of erosion on the delta deposit can be interpreted from the surface shear stress (A/B), and largest grain sizes that could be mobilized by typical winds (C/D). Large eddy simulation was conducted on the delta deposit topography (E) to model surface shear from easterly (A) and southwesterly (B) winds. Several locations of high shear stress (white boxes), a proxy erosion potential, are within the landing ellipse. Erosion can only proceed if sand grains are moved by the wind. Estimates of mobile grain sizes derived from the simulations suggest medium-grained sand could be mobilized across much of the delta front (C/D).

the front of the eroded delta deposit meets the basal plains. These upwind-facing slopes, therefore, represent locations where erosion would have had the potential to be most rapidly occurring when the modeled wind was present. However, wind-driven erosion requires available sediment; mobile sands, not the air itself, are responsible for the actual erosion by abrasion (Powers, 1936; Suzuki & Takahashi, 1981). Actively migrating sands are relatively rare within Jezero crater, but locations where active transport has been documented coincide with the high-shear stress regions modeled in this work (Chojnacki et al., 2018). We used the results of the large eddy simulation to determine the largest grain sizes mobilized by typical winds on Mars. In the regions of highest shear stress, we found that wind is expected to mobilize medium-grained sand (Figs. 2c,d). Satellite imaging has shown changes in the dark sands at the delta front (Chojnacki et al., 2018). Assuming these sands are similar in grain-size to active sands imaged by the Mars Science Laboratory rover (i.e., fine to medium; Weitz et al., 2018), results of this work suggest these grains are likely mobile in typical martian winds.

Areas of high shear stress are spread across the delta, but those far from the landing ellipse present practical difficulties by requiring a further rover traverse. For this reason, below we discuss three specific areas of high shear stress that are 1) near sediments that could be entrained by wind to cause modern abrasion, and 2) within or close to within the landing ellipse (Figs. 3-5).

4 Discussion

4.1 Sediment availability and traversability hazards

Aeolian erosion only occurs when mobile sand is present (Powers, 1936; Suzuki & Takahashi, 1981). In Jezero crater, two types of bedforms could potentially provide sands and enable wind-driven erosion. The dominant bedforms in the study area and Jezero crater at large are straight-crested transverse aeolian ridges (Berman et al., 2011; Zimbelman, 2010). These bright-looking bedforms are commonly found in topographic lows and are decameters in length. The second type of bedforms in the study area are “large martian ripples” (Lapotre et al., 2016, 2018). These meter-scale bedforms develop more complex patterns than their straight-crested neighbors, and are typically dark in satellite images. Unlike the larger bright bedforms that occur as separated and parallel features, the dark ripples occur on sand sheets with continuous coverage. Previous research has shown that these dark ripples are actively being transported by the wind (Chojnacki et al., 2018). Conversely, the bright bedforms appear inactive and have not changed position in the last ~10 years. This inactivity suggests that the sand in these bedforms is not available to be entrained by the wind, and even though the bright bedforms are abundant, they may not provide sediment for erosion. Grain size distributions within or armoring the bedforms could account for the apparent differences in activity over time. The grain size values shown in Figure 2 provide upper limits on the grains in mobile bedforms, and lower limits on the surface grains of immobile bedforms.

Bedforms in the study area also present a practical difficulty for the rover. Dunes, ripples, and related accumulations of sand can be difficult for wheeled rovers to traverse. The two Mars Exploration Rovers, *Opportunity* and *Spirit*, both became trapped in wind-blown ripples, ultimately ending the mission of *Spirit* (Greeley et al., 2008; Sullivan et al., 2005). The Mars Science Laboratory rover *Curiosity* also encountered mobility issues in wind-blown bedforms (Rothrock et al., 2016), but was able to traverse a large bright bedform with little difficulty

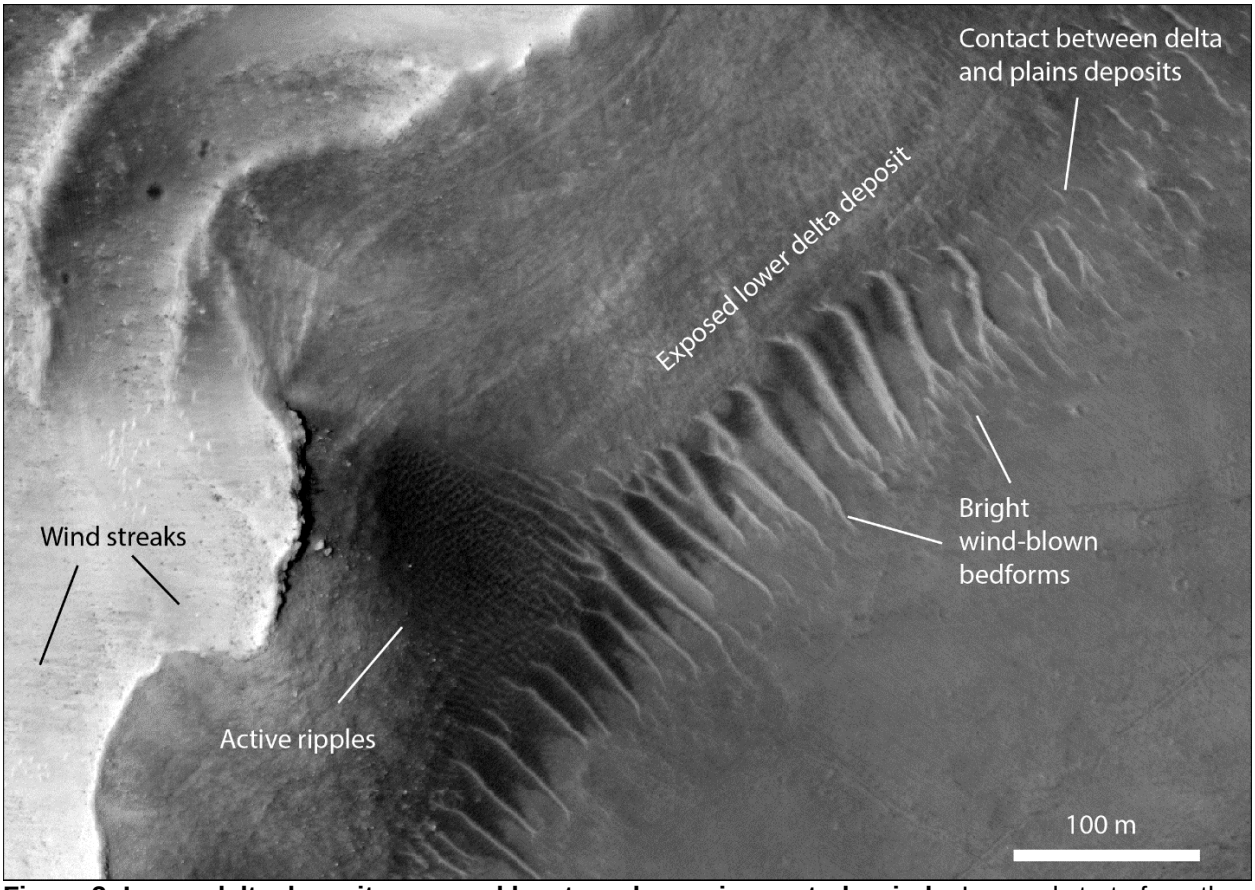

Figure 3: Lower delta deposits exposed by strongly erosive easterly winds. Layered strata from the delta deposit are evident on the sloping surface above smooth plains covered in active and inactive bedforms that concentrate near the change in topography. Here the contact between the delta and plains deposits could be accessed by a rover. ESP_042315_1985.

(Arvidson et al., 2017). The aeolian bedforms in Jezero crater share characteristics with the bedforms that challenged the *Curiosity* rover and the bedform it traversed, making the trafficability of these features uncertain. Regardless, understanding wind-blown sands as both a scientific tool and an engineering hazard will be critical to successfully collecting samples that optimize the chances of detecting ancient martian life.

4.2 Optimal sampling sites for Mars Sample Return

Based on the results of large eddy simulations, three areas near the rover landing ellipse have experienced high shear stresses, and are locations where strata may have been recently exposed by easterly or southwesterly winds. To date, it remains unclear which winds have most recently eroded material from the delta deposit. Given the amount of material interpreted to have been removed (Goudge et al., 2017), it is expected that upon landing the rover will encounter a landscape that has been highly abraded. The millimeter- to decimeter-scale patterns of this abrasion, not resolvable in satellite images, will provide evidence of sand-transporting, erosive winds and will enable differentiation between the models shown here (Bridges et al., 2004, 2014).

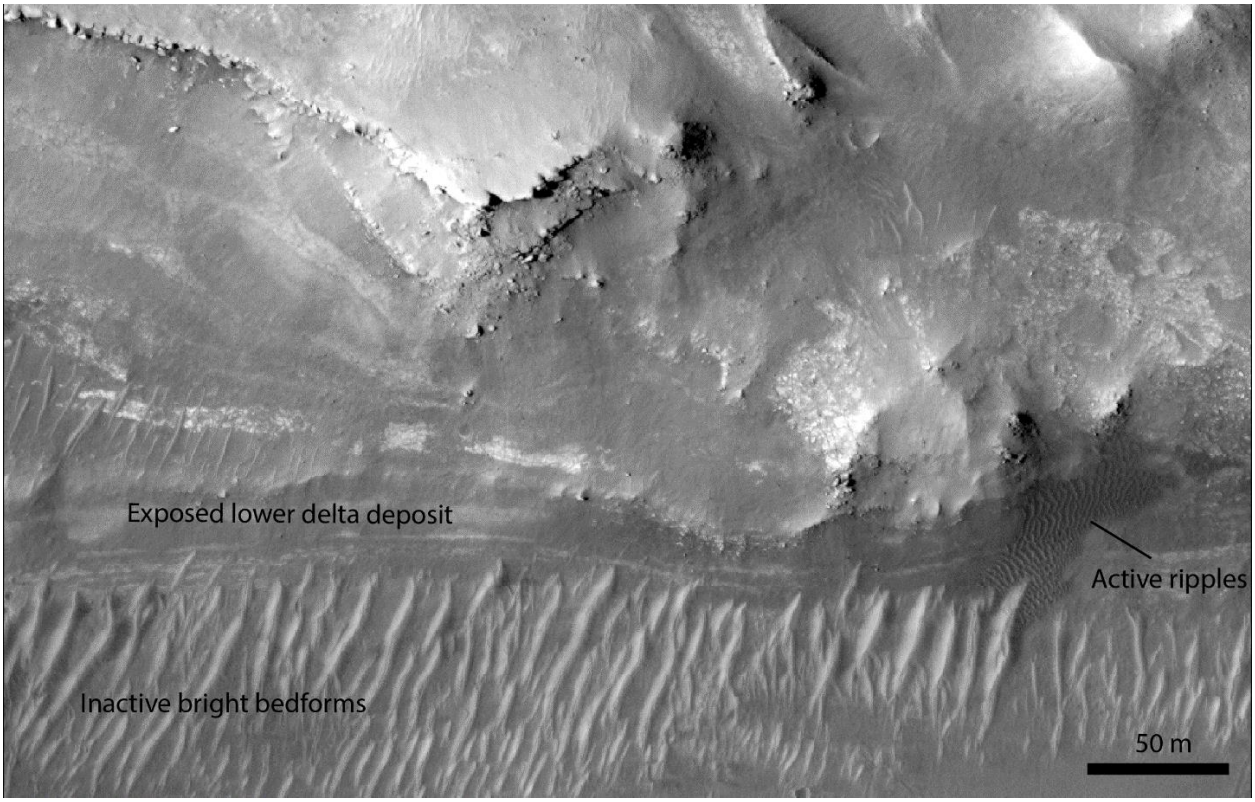

Figure 4: Lower delta deposits exposed by strongly erosive southwesterly winds. Lower delta strata exposed in this area show striking light-toned layers. Active and inactive bedforms cover the smooth plains at the base of the slope. ESP_037396_1985.

A high-priority target for sampling will be the basal strata in the delta deposit. Although material higher in the delta is also of interest, basal and distal portions of the deposit are most likely to house any fine-grained organic material emplaced during the formation of the delta. Figure 3 shows basal delta deposits exposed on a slope that would have experienced high surface stresses from easterly winds. Layering in this slope is juxtaposed with active sands from a small ripple field climbing the exposed face. Dark and light bedforms impede slope access, but bedrock can be seen between the larger straight-crested bedforms. In the northeast portion of this potential sampling area, the bedforms become sparser and delta strata can be followed from the deposit to the contact with the underlying plains, thus providing confidence that the delta strata could be easily accessed by the rover. On the upper surface of the delta, thin wind streaks record easterly winds, consistent with previous works.

Basal delta deposits are also exposed on a face that would be eroded under southwesterly winds (Fig. 4). Again, active and inactive bedforms are juxtaposed at the base of the deposit, suggesting that some sediment would be available to cause erosion. Strata within the deposit include light-tone beds, potentially associated with clay minerals previously identified in the region (Ehlmann et al., 2008; Goudge et al., 2015). A field of inactive light bedforms sits along the base of the exposed face, obscuring the transition from delta strata to plains. Bedforms in this area are more varied in size, obscuring more of the inter-bedform space and potentially posing difficulties for mobility.

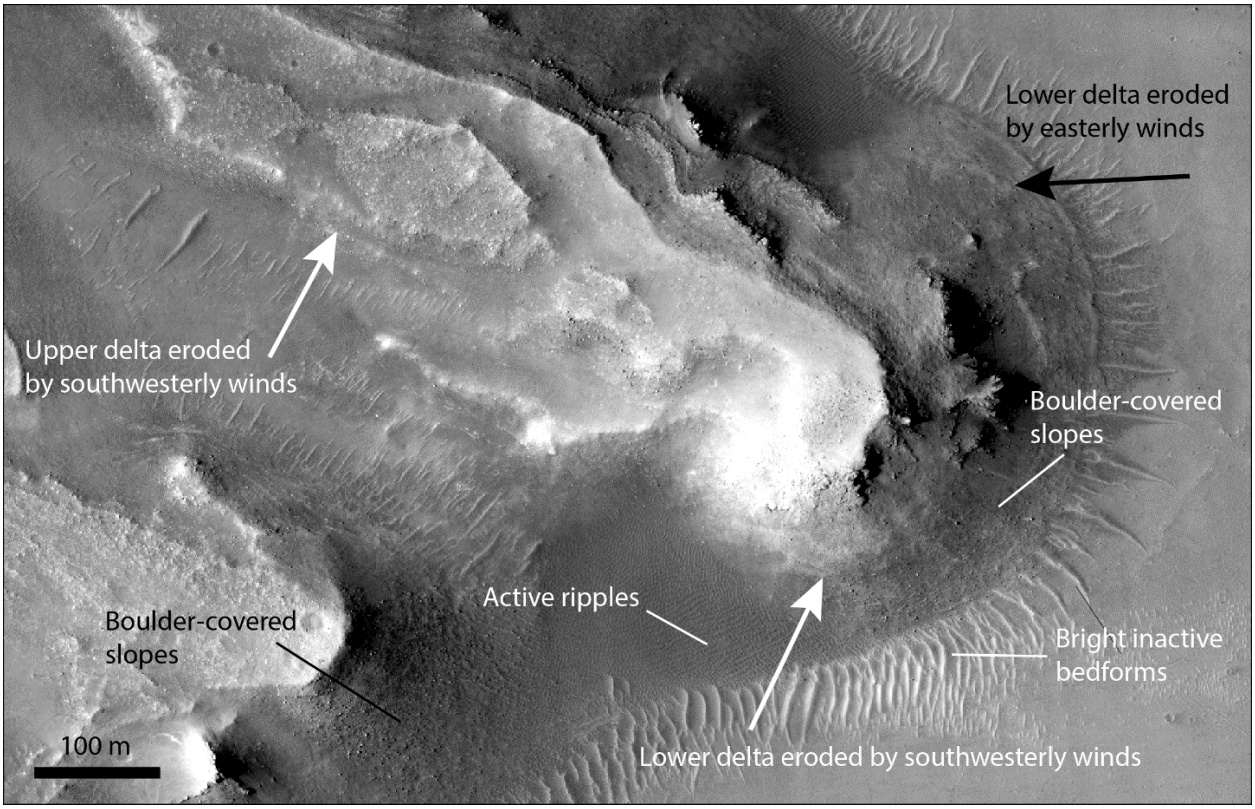

Figure 5: Delta strata eroded by easterly and southwesterly winds in close proximity. This protruding outcrop of delta strata includes areas that would have been rapidly eroded by southwesterly winds (white arrows) and easterly winds (black arrow). Both lower and upper delta strata are accessible here. Active and inactive bedforms are present along the base of the slope. Boulders and loose cover obscure the strata in the slope itself. ESP_037330_1990.

Given that it remains unclear which winds caused the most recent erosion, there are practical benefits to locations where strata are exposed in multiple orientations. Such locations also provide opportunities to observe the three-dimensional geometry of the delta. The region shown in Figure 5 includes portions of the delta deposit that experience high surface shear stresses from both easterly and southwesterly winds (Fig. 2). As elsewhere, dark, active ripples are juxtaposed with bright bedforms at the base of the delta deposit. The large bedforms are oriented normal to the slope, such that a rover could drive between bedforms, however, bedform spacing and inter-bedform sediment cover varies, with sediment cover decreasing to the north. This location provides access to both lower and upper strata in the delta deposit. In the simulation of southwesterly winds, both lower and upper delta strata experience high surface shear stresses. Lower delta strata in this area are less clearly exposed. Boulders on the slope suggest mass wasting; material from the overlying units may cover the lowermost strata. This is counter to the idea that this material has been recently eroded by wind. The goal of this work is not to identify a perfect target for exploration, but rather to discuss the available options in the context of surface-wind interactions.

4. 3 Geology augmenting meteorology

Measurements of the modern wind will be collected by the Mars Environmental Dynamics Analyzer (MEDA) onboard the *Perseverance* rover (Rodriguez-Manfredi et al., 2014).

Although these measurements will provide a helpful characterization of the local turbulent winds, measurements from MEDA alone are insufficient to identify locations of recent erosion. Erosion requires mobile sand, and the threshold wind speeds at which sand saltation is initiated on Mars are not fully understood (Baker et al., 2018; Kok, 2010; Sullivan & Kok, 2017). Day-to-day winds in Jezero crater may or may not transport sediment, and even if daily winds can be demonstrated to move sand, the current availability of sediment may not be sufficient to cause erosion. Furthermore, winds vary in speed and direction both spatially and temporally (Day & Rebolledo, 2019; Haberle et al., 1993; Leovy & Mintz, 1969; Thomas & Veverka, 1979). It will take the full duration of the primary mission to characterize the seasonal variations in surface winds using MEDA, and to determine whether and where modern winds cause erosion. By that time, any results will be too late to be applied to mission planning and sample site selection. Therefore, basing interpretations and sampling decisions on the observed surface geology, which necessarily reflects sand-transporting winds, will provide a rapid and rigorous characterization of the recent wind history critical to identifying recently exposed outcrops and maximizing the potential to identify evidence of early life on Mars.

Acknowledgments

The authors thank Kate Ledger for editorial contributions to this work. Data availability statement: Data used in this work is archived online at https://github.com/GALE-Lab/Day-Anderson-SubmittedToGRL.

References

Albertson, J. D., & Parlange, M. B. (1999). Surface length scales and shear stress: Implications for land-atmosphere interaction over complex terrain. Water Resources Research, 35(7), 2121–2132.

Anderson, R. S., Sørensen, M., & Willetts, B. B. (1991). A review of recent progress in our understanding of aeolian sediment transport. In Aeolian Grain Transport 1 (pp. 1–19). Springer.

Anderson, W. (2013). An immersed boundary method wall model for high-Reynolds-number channel flow over complex topography. International Journal for Numerical Methods in Fluids, 71(12), 1588–1608.

Anderson, W., & Day, M. (2017). Turbulent flow over craters on Mars: Vorticity dynamics reveal aeolian excavation mechanism. Physical Review E, 96(4), 43110. Retrieved from https://link.aps.org/doi/10.1103/PhysRevE.96.043110

Anderson, W., & Meneveau, C. (2010). A large-eddy simulation model for boundary-layer flow over surfaces with horizontally resolved but vertically unresolved roughness elements. Boundary-Layer Meteorology, 137(3), 397–415.

Arvidson, R. E., Iagnemma, K. D., Maimone, M., Fraeman, A. A., Zhou, F., Heverly, M. C., et al. (2017). Mars Science Laboratory Curiosity rover megaripple crossings up to sol 710 in Gale Crater. Journal of Field Robotics, 34(3), 495–518.

Baker, M. M., Newman, C. E., Lapotre, M. G. A., Sullivan, R., Bridges, N. T., & Lewis, K. W. (2018). Coarse Sediment Transport in the Modern Martian Environment. Journal of

Geophysical Research: Planets, 123(6), 1380–1394. https://doi.org/10.1002/2017JE005513

Banfield, D., Spiga, A., Newman, C., Forget, F., Lemmon, M., Lorenz, R., et al. (2020). The atmosphere of Mars as observed by InSight. Nature Geoscience, 1–9.

Berman, D. C., Balme, M. R., Rafkin, S. C. R., & Zimbelman, J. R. (2011). Transverse aeolian ridges (TARs) on Mars II: distributions, orientations, and ages. Icarus, 213(1), 116–130.

Bridges, N. T., Laity, J. E., Greeley, R., Phoreman, J., & Eddlemon, E. E. (2004). Insights on rock abrasion and ventifact formation from laboratory and field analog studies with applications to Mars. Planetary and Space Science, 52(1), 199–213. https://doi.org/10.1016/j.pss.2003.08.026

Bridges, N. T., Kocurek, G. A., Langevin, Y., Lewis, K. W., Mangold, N., Maurice, S., et al. (2014). The rock abrasion record at Gale Crater: Mars Science Laboratory results from Bradbury Landing to Rocknest. Journal of Geophysical Research - Planets, 119(6), 1374–1389. https://doi.org/10.1002/2013je004579

Chojnacki, M., Banks, M., & Urso, A. (2018). Wind-Driven Erosion and Exposure Potential at Mars 2020 Rover Candidate-Landing Sites. Journal of Geophysical Research: Planets, 123(2), 468–488.

Dartnell, L. R., Desorgher, L., Ward, J. M., & Coates, A. J. (2007). Modelling the surface and subsurface Martian radiation environment: Implications for astrobiology. Geophysical Research Letters, 34(2), L02207. https://doi.org/10.1029/2006gl027494

Dartnell, L. R., Patel, M. R., Cockell, C., Burchell, M., & Martins, Z. (2014). Degradation of microbial fluorescence biosignatures by solar ultraviolet radiation on Mars. International Journal of Astrobiology, 13(2), 112–123. https://doi.org/10.1017/s1473550413000335

Day, M., & Dorn, T. (2019). Wind in Jezero crater, Mars. Geophysical Research Letters, 46(6), 3099–3107.

Day, M., & Rebolledo, L. (2019). Intermittency in Wind-Driven Surface Alteration on Mars Interpreted From Wind Streaks and Measurements by InSight. Geophysical Research Letters, 46(22), 12747–12755.

Day, M., Anderson, W., Kocurek, G., & Mohrig, D. (2016). Carving intracrater layered deposits with wind on Mars. Geophysical Research Letters, 43(6), 2473–2479. https://doi.org/10.1002/2016gl068011

Ehlmann, B. L., Mustard, J. F., Fassett, C. I., Schon, S. C., Head III, J. W., Marais, D. J. Des, et al. (2008). Clay minerals in delta deposits and organic preservation potential on Mars. Nature Geoscience, 1(6), 355–358.

Fassett, C. I., & Head, J. W. (2005). Fluvial sedimentary deposits on Mars: Ancient deltas in a crater lake in the Nili Fossae region. Geophysical Research Letters, 32(14).

Greeley, R., Whelley, P. L., Neakrase, L. D. V, Arvidson, R. E., Bridges, N. T., Cabrol, N. A., et al. (2008). Columbia Hills, Mars: Aeolian features seen from the ground and orbit. Journal of Geophysical Research - Planets, 113(E6).

Goudge, T. A., Mustard, J. F., Head, J. W., Fassett, C. I., & Wiseman, S. M. (2015). Assessing the mineralogy of the watershed and fan deposits of the Jezero crater paleolake system, Mars. Journal of Geophysical Research: Planets, 120(4), 775–808.

Goudge, T. A., Mohrig, D., Cardenas, B. T., Hughes, C. M., & Fassett, C. I. (2017). Stratigraphy and Evolution of Delta Channel Deposits, Jezero Crater, Mars.

Haberle, R. M., Pollack, J. B., Barnes, J. R., Zurek, R. W., Leovy, C. B., Murphy, J. R., et al. (1993). Mars atmospheric dynamics as simulated by the NASA Ames General

Circulation Model: 1. The zonal-mean circulation. Journal of Geophysical Research: Planets, 98(E2), 3093–3123.

Kok, J. F. (2010). An improved parameterization of wind-blown sand flux on Mars that includes the effect of hysteresis. Geophysical Research Letters, 37(12). https://doi.org/10.1029/2010gl043646

Kok, J. F. (2010). Analytical calculation of the minimum wind speed required to sustain wind-blown sand on Earth and Mars. Geophysical Research Letters, 37(L12202).

Lapotre, M. G. A., Ewing, R. C., Lamb, M. P., Fischer, W. W., Grotzinger, J. P., Rubin, D. M., et al. (2016). Large wind ripples on Mars: A record of atmospheric evolution. Science, 353(6294), 55–58. https://doi.org/10.1126/science.aaf3206

Lapotre, M. G. A., Ewing, R. C., Weitz, C. M., Lewis, K. W., Lamb, M. P., Ehlmann, B. L., & Rubin, D. M. (2018). Morphologic diversity of Martian ripples: Implications for large-ripple formation. Geophysical Research Letters, 45(19), 10–229.

Leovy, C., & Mintz, Y. (1969). Numerical simulation of the atmospheric circulation and climate of Mars. Journal of the Atmospheric Sciences, 26(6), 1167–1190.

Martin, R. L., & Kok, J. F. (2017). Wind-invariant saltation heights imply linear scaling of aeolian saltation flux with shear stress. Science Advances, 3(6). https://doi.org/10.1126/sciadv.1602569

McEwen, A. S., Eliason, E. M., Bergstrom, J. W., Bridges, N. T., Hansen, C. J., Delamere, W. A., et al. (2007). Mars Reconnaissance Orbiter's High Resolution Imaging Science Experiment (HiRISE). Journal of Geophysical Research: Planets, 112(E5). https://doi.org/10.1029/2005je002605

Meneveau, C., & Katz, J. (2000). Scale-invariance and turbulence models for large-eddy simulation. Annual Review of Fluid Mechanics, 32(1), 1–32. https://doi.org/10.1146/annurev.fluid.32.1.1

Pope, S. B. (2000). Turbulent flows. Cambridge: Cambridge University Press.

Powers, W. E. (1936). The evidences of wind abrasion. The Journal of Geology, 44(2, Part 1), 214–219.

Rodriguez-Manfredi, J. A., de la Torre, M., Conrad, P., Lemmon, M., Martinez, G., Newman, C., et al. (2014). MEDA: an environmental and meteorological package for Mars 2020. In Lunar and Planetary Science Conference (Vol. 45, p. 2837).

Rothrock, B., Kennedy, R., Cunningham, C., Papon, J., Heverly, M., & Ono, M. (2016). Spoc: Deep learning-based terrain classification for mars rover missions. In AIAA SPACE 2016 (p. 5539).

Salvatore, M. R., Goudge, T. A., Bramble, M. S., Edwards, C. S., Bandfield, J. L., Amador, E. S., et al. (2018). Bulk mineralogy of the NE Syrtis and Jezero crater regions of Mars derived through thermal infrared spectral analyses. Icarus, 301, 76–96.

Schon, S. C., Head, J. W., & Fassett, C. I. (2012). An overfilled lacustrine system and progradational delta in Jezero crater, Mars: Implications for Noachian climate. Planetary and Space Science, 67(1), 28–45.

Shao, Y., & Lu, H. (2000). A simple expression for wind erosion threshold friction velocity. Journal of Geophysical Research, 105(D17), 22437–22443. https://doi.org/10.1029/2000jd900304

Sullivan, R., & Kok, J. F. (2017). Aeolian saltation on Mars at low wind speeds. Journal of Geophysical Research: Planets, 122(10), 2111–2143. https://doi.org/10.1002/2017je005275

Sullivan, R., Banfield, D., Bell, J., Calvin, W., Fike, D., Golombek, M., et al. (2005). Aeolian processes at the Mars Exploration Rover Meridiani Planum landing site. Nature, 436(7047), 58–61. https://doi.org/10.1038/nature03641

Suzuki, T., & Takahashi, K. (1981). An experimental study of wind abrasion. The Journal of Geology, 89(1), 23–36.

Thomas, P., & Veverka, J. (1979). Seasonal and secular variation of wind streaks on Mars: An analysis of Mariner 9 and Viking data. Journal of Geophysical Research: Solid Earth, 84(B14), 8131–8146.

Weitz, C. M., Sullivan, R. J., Lapotre, M. G. A., Rowland, S. K., Grant, J. A., Baker, M., & Yingst, R. A. (2018). Sand grain sizes and shapes in eolian bedforms at Gale crater, Mars. Geophysical Research Letters, 45(18), 9471–9479.

Wyngaard, J. C. (2010). Turbulence in the Atmosphere. Cambridge University Press.

Zimbelman, J. R. (2010). Transverse Aeolian Ridges on Mars: First results from HiRISE images. Geomorphology, 121(1), 22–29. https://doi.org/10.1016/j.geomorph.2009.05.012